# Validation of the NPARC Code in Supersonic Base Flows

P. I. Espina*
*National Institute of Standards and Technology*
*Gaithersburg, Maryland 20899*

and

U. Piomelli†
*University of Maryland*
*College Park, Maryland 20742*

## Abstract

The supersonic annular flow over the base of a circular cylinder was used to validate the axisymmetric version of the NPARC code in a flow with large separated regions, attached flow regions, and free shear layers. Numerical results obtained using adaptive grids were compared to an extensive experimental database that includes turbulence information in the base region of the flow. The original NPARC code was modified to include a more faithful implementation of the original Baldwin-Lomax turbulence model. In addition, numerical results were obtained using a compressible version of the $k$-$\epsilon$ model by Chien and a newly added $k$-$\epsilon$ model by Grasso & Falconi. In general, the two-equation models predicted more accurately the overall features in the base flow than the zero-equation models, although all models had difficulty predicting the base pressure. The results showed that the location of the reattachment point is strongly influenced by the outer jet structure, which has typically been ignored in previous base-type flow investigations.

## Nomenclature

| | |
|---|---|
| $k$ | turbulence kinetic energy |
| $\epsilon$ | turbulence dissipation rate |
| $M$ | Mach number |
| $P$ | pressure |
| $T$ | temperature |
| $\gamma$ | specific heat ratio |
| $R$ | base radius $= 31.75\ mm$ |
| $y$ | wall normal coordinate |
| $R_\theta$ | momentum thickness Reynolds Number |
| $u$ | streamwise velocity |
| $u_\tau$ | friction velocity |
| $\nu$ | kinematic viscosity |
| $\nu_t$ | eddy viscosity |

*Subscripts*

| | |
|---|---|
| $e$ | nozzle exit |
| $r$ | receiving chamber |
| $exit$ | wind tunnel exit |
| $\infty$ | conditions at infinity |
| $wall$ | conditions at the wall |
| $b$ | conditions at the base |

*Superscripts*

| | |
|---|---|
| $+$ | based on wall units |

## Introduction

Axisymmetric base flows have been extensively studied during the last four decades, primarily due to their importance in ballistic problems. In this type of flow, the need to achieve an understanding of the mechanisms that yield reduced pressures at the tails of bullets and missiles has led to theoretical,[1−3] numerical,[4−9] and experimental[10] investigations (reviews of the pertinent literature can be found in references 3, 9 and 10). In all cases, attempts have been made to determine ways to control the flow structure in the wake region such that base drag is reduced and vehicle stability is increased.

The basic structure of the supersonic base-flow is also at the heart of the materials-processing device known as the *gas-metal atomizer*. In this device, an orifice is placed at the center of the base while an annular gas jet flows around it. Liquid metal is allowed to flow through the orifice into the reduced

*Mechanical Engineer, Fluid Flow Group, Bldg. 230, Rm. 105. Student Member AIAA.

†Associate Professor, Department of Mechanical Engineering. Senior Member AIAA.

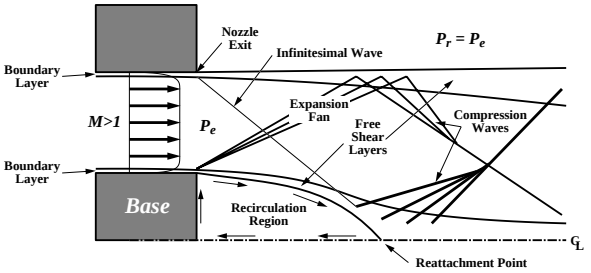


Figure 1. Schematic of the axisymmetric base flow produced by the flow of a supersonic annular jet over the end of a circular cylinder.

pressure region at the base, and the exchange of momentum between the gas and liquid phases induces instabilities in the liquid which lead to its disruption. Typically, the disruption process continues until the droplets attain a Weber number small enough to preclude further disruption. They then solidify in flight. At the end of the process, the gas-powder mixture is separated and parts are sintered from the powder in post-processing operations.

In an atomizer, control of the base pressure is of utmost importance given that this parameter controls the flow rate of the liquid metal to be processed. The ultimate goal of the materials industry is to produce metal powders of known particle-size distributions with the least amount of gas and at the lowest jet stagnation pressure possible. Therefore, this investigation deviates from the previous base-flow research in that its motivation is to determine mechanisms with which to *control* the base drag.

The base flow structure that results as a supersonic annular jet surrounds the end of a circular cylinder at *design* pressure ratio is schematically shown in Figure 1. When the flow emanating from the nozzle encounters the end corner of the cylinder, it undergoes an expansion process to satisfy the surface-angle change imposed by the termination of the cylinder. The flow separates and forms a free shear layer that propagates towards the axis of symmetry of the geometry. The resulting internal shear layer encapsulates a volume of low-speed fluid in the area downstream of the base of the cylinder. At the axis of symmetry, the flow is forced to compress through a series of compression waves to change its direction. The resulting outbound-propagating compression waves collapse into a curved shock wave that propagates away from the axis of symmetry. Meanwhile, the expansion waves generated in the initial expansion fan propagate towards the outer free shear layer of the jet from which they reflect as compression waves. These waves then collapse into a single curved shock wave that propagates towards the axis of symmetry. Both resulting shock waves will continue to interact further downstream to form a complex jet structure.

Flows similar to the one described above have been studied theoretically and numerically in the past. In references 1–3, Mueller *et al.* studied the effects of geometry and pressure ratio on base pressure for plug nozzles. Based on experimental data and theoretical considerations, they derived a model capable of predicting the pressure at the base in a number of geometries. In reference 4, Mikhail *et al.* present the study of the base flow behind the AGARD 10-deg. nozzle with mass injection at the base. Their results were computed using a $30 \times 39$ mesh, which led to poor spatial resolution in the data. In references 5–7, Sahu and co-workers present results for flows over a variety of boattail configurations (with and without mass injection) using a number of different numerical methods. Peace[8] studied three variations of a circular-arc boattail with mass injection by solving the Navier-Stokes equations with the Baldwin-Lomax and Chien's $k$-$\epsilon$ turbulence models. His results, which took advantage of grid adaptation methods, revealed that the $k$-$\epsilon$ predictions are superior to those obtained using the Baldwin-Lomax model. He found good agreement between the numerical and experimental results for attached flow configurations, but both models had trouble predicting the physics of separated flow regions.

Recently, a detailed experimental description of the flow structure in the base area of a cylinder engulfed by a supersonic stream was given by Herrin & Dutton.[10] Their data are the first to contain detailed three-dimensional velocity and turbulence information in the base region obtained by non-intrusive methods. The availability of these data has spawned numerical investigations by Sahu *et al.*[7] and Tucker *et al.*,[9] who performed almost identical studies of the flow structure in the base region.

In this investigation, we focus on the validation of numerical techniques to simulate the gas-only flow in gas-metal atomizers by simulating the complete flow field studied by Herrin & Dutton.[10] Although the aforementioned numerical investigations[7,9] have studied this test case, they restricted their findings to the near-wake region and gave little detail of the outer jet region, which is of importance in atomization flows.

The results presented here document the dif-

ferences between the predictions obtained using the zero-equation turbulence model by Baldwin-Lomax[11] and the two-equation turbulence models by Chien[12] (as implemented by Georgiadis *et al.*[13]) and by Grasso & Falconi.[14] Also discussed are a few modifications to the NPARC code[15] dealing with the implementation of the Baldwin-Lomax model. In addition, this work analyzes the base-flow structure that results when the annular gas jet is operated at off-design pressure ratios; emphasis is placed on under-expanded pressure ratios that encompass the predominant regime at which gas-metal atomizers are operated.

## Numerical Method

### Governing Equations

The axisymmetric, steady, compressible flow in the wake of a cylindrical afterbody is governed by the nonreacting Navier-Stokes equations. In this work, the Navier-Stokes equations are solved in strong, conservative form in a curvilinear coordinate system. The fluid is assumed to be a thermally- and calorically-perfect gas that exhibits a Newtonian stress-strain behavior. Thermal conductivity is taken to be identical to the molecular viscosity, which is related to the static temperature by the Sutherland viscosity law.

### Numerical Algorithm

The solution to the Navier-Stokes equations was accomplished using the NPARC code,[15] based on the ARC2D algorithm.[16] In this algorithm, time advancement is performed using a backward Euler scheme. Approximate factorization is used to facilitate solution of the resulting system of equations, and both second- and fourth-order artificial dissipation are introduced to suppress dispersion errors near shock waves and decoupling of even-odd modes due to the central difference discretization. The resulting equation yields a series of block pentadiagonal systems that can be linearized by time-advancing the viscous fluxes and the axisymmetric source terms explicitly. This results in a series of scalar pentadiagonal systems that are solved directly using the Thomas algorithm.

### Turbulence Models

Solutions of the axisymmetric base flow were obtained using: (1) the NPARC implementation[15] of the Baldwin-Lomax[11] model, (2) a more faithful implementation of the Baldwin-Lomax model,

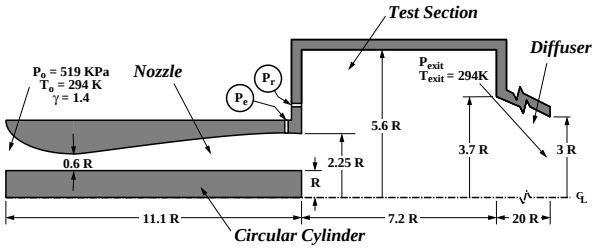


Figure 2. Schematic diagram of the computational domain used in the base-flow problem.

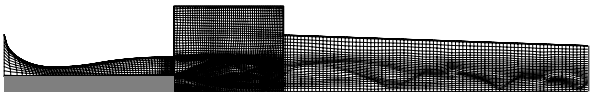

Figure 3. Computational mesh adapted for simulation of base flow at the designed pressure ratio (only every fourth grid line is shown for clarity).

(3) a compressible implementation[13] of Chien's[12] $k$-$\epsilon$ model, and (4) Grasso & Falconi's[14] $k$-$\epsilon$ turbulence model. For the $k$-$\epsilon$ models, the solution to the turbulence equations was time-lagged with respect to the solution of the flow equations and was accomplished using the algorithm suggested by Sahu and Danberg.[17] In this algorithm, second-order, upwind differences are used to approximate the spatial derivatives, and approximate factorization is used to facilitate solution of the resulting equation. This renders the use of artificial dissipation unnecessary, given the inherent smoothing properties of the upwind differences. The resulting equation yields a series of block tridiagonal systems that are solved directly using a block version of the Thomas algorithm.

### Physical Domain and Boundary Conditions

The computational domain used in this investigation (see Figure 2) follows the specifications of the supersonic tunnel used by Herrin & Dutton[10] as given in references 18 and 19. The tunnel domain was segmented into three separate grids: the nozzle ($266 \times 81$ points in the axial and radial directions respectively), the test section ($255 \times 279$), and the diffuser ($338 \times 125$). Within each block, the mesh points were distributed using the SAGE[20] grid adaptation program. At all solid boundaries, the first line of points parallel to the wall was forced to be located at $y^+ \leq 1$ to obtain accurate resolution at the wall layer. The final adapted grid used in one of the tested flows is shown in Figure 3.

Characteristic type boundary conditions were used at the inlet of the nozzle ($P_o$, $T_o$ specified) and

at the outlet of the diffuser ($P_{exit}$, $T_{exit}$ specified). The interfaces between the nozzle and the test section blocks as well as between the test section and the diffuser blocks were interpolated explicitly. Axisymmetry was used at the axes of the test section and the diffuser blocks while all other boundaries were treated as adiabatic, non-slip walls.

### Modifications to the NPARC code

As part of this investigation, two modifications were made to the original NPARC algorithm in an attempt to improve the quality of the computed results: (1) the implementation of the Baldwin-Lomax model, and (2) the addition of the compressible $k$-$\epsilon$ turbulence model by Grasso & Falconi. What follows describes these modifications in some detail.

**Baldwin-Lomax Model.** Results obtained for the base flow problem showed that the NPARC implementation of the Baldwin-Lomax model yielded discontinuous streamwise eddy viscosity distributions. These were mostly due to problems in the evaluation of the crossover distance between the outer and inner model formulations.[11] Furthermore, as implemented in the NPARC code, the model makes no provisions for the generation of turbulent stresses unless a wall is present. This leads to problems if one desires to model free flows such as shear layers and jets for which the model would yield zero eddy viscosity.

In an attempt to improve the performance of the model, a number of modifications were implemented. First, the outer model formulation was added to the axisymmetric boundary condition (i.e., type 51) and to a new two-dimensional symmetry boundary condition (i.e., type 52) as recommended in the original Baldwin-Lomax paper for the simulation of wakes.[11] This allows for the production of turbulence stresses in free flows by replacing the wall normal distance by a length scale derived from the local value of the vorticity. Secondly, in the NPARC implementation, the eddy viscosity is defined as the minimum value obtained from either the inner or outer formulations of the Baldwin-Lomax model. This works adequately only if the eddy viscosity distributions given by both formulations vary monotonically away from the wall which is not always the case. For this work, we followed the criteria given in Reference 11 which sets a crossover distance after which the inner model formulation is replaced by the outer model. Finally, the eddy viscosity was processed through a trapezoidal filter to remove any discontinuities not removed by the other modifications. During testing, the use of this filtering stage did not prove to be absolutely necessary and given its dissipative nature, one may choose to remove it. Nonetheless, the filter was used in the results that follow.

**Grasso & Falconi's $k$-$\epsilon$ Model.** The Grasso & Falconi's $k$-$\epsilon$ model[14] differs from the compressible version of Chien's model in: (a) the addition of the pressure-dilatation, dilatation-dissipation, and Favre-velocity contribution terms to the RHS of the $k$ equation which are meant to account for the production of $k$ due to compressibility effects, (b) the subtraction of the near-wall terms used in Chien's model to allow for the non-physical declaration of $\epsilon_{wall} = 0$, and (c) the values of the proportionality constants. The reader is referred to references 12–14 for details on both models.

## Results

### Boundary Layer Flow

Prior to the simulation of the base flows, the turbulence models were tested by simulating the boundary layer over a flat plate with zero pressure gradient at free stream Mach numbers of: 0.2, 1.2, and 4.0. Figure 4 compares the compressible law of the wall ($u^+ = y^+$, for $y^+ < 10$; $u^+ = \log y^+/0.41 + 5$, for $y^+ > 10$) with the streamwise velocity predictions obtained using direct numerical simulation (DNS),[21] and the results of four eddy-viscosity turbulence models for $M_\infty = 0.2$, $R_\theta = 1410$.

As seen in the figure, both the original and the NPARC implementation of the Baldwin-Lomax model predicted the DNS data with satisfactory accuracy, yielding a value of $u_\tau$ only 3% lower than its DNS counterpart. Both models gave almost identical results due to the fact that the modifications made to the NPARC model do not affect the results for wall bounded flows like this boundary layer. The small difference between the two models resulted from the use of the trapezoidal filter in the original model which tends to smear flow features due to its dissipative nature. For both models, the eddy viscosity predictions present a discontinuity at $y^+ \approx 85$ due to the switch between the inner and outer formulations of the models (see Figure 5, top).

Chien's $k$-$\epsilon$ model performed extremely well in the boundary layer flow with a deviation in the value of $u_\tau$ of only 0.9% from the DNS results (see Figure 4). Figure 5 shows that this model gives a continuous distribution of eddy viscosity and a prediction

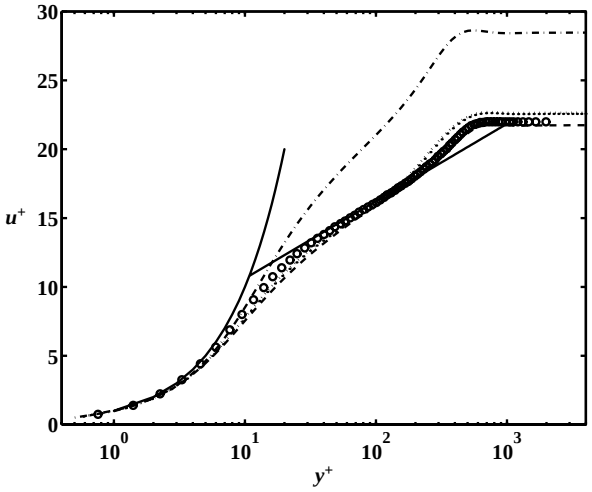


Figure 4. Effect of turbulence model on the streamwise velocity distribution of a boundary layer, $R_\theta = 1410$, $M_\infty = 0.2$. ——— : law of the wall; ∘ : DNS; – – – : Chien's $k$-$\epsilon$; –·–·– : Grasso & Falconi's $k$-$\epsilon$; ····· : NPARC's Baldwin-Lomax; ····· : original Baldwin-Lomax.

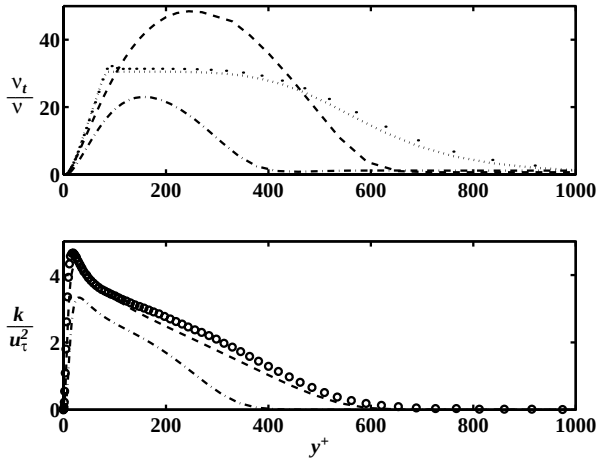


Figure 5. Effect of turbulence model on turbulence parameters of a boundary layer, $R_\theta = 1410$, $M_\infty = 0.2$. (Top) eddy viscosity distribution, – – – : Chien's $k$-$\epsilon$; –·–·– : Grasso & Falconi's $k$-$\epsilon$; ····· : NPARC's Baldwin-Lomax; ····· : original Baldwin-Lomax. (Bottom) turbulent kinetic energy distribution, ∘ : DNS; – – – : Chien's $k$-$\epsilon$; –·–·– : Grasso & Falconi's $k$-$\epsilon$.

of turbulent kinetic energy almost identical to that of the DNS. In contrast, the results obtained using the Grasso & Falconi model underpredicted the friction velocity by 33% and yielded an estimate of eddy viscosity that is about two thirds of that obtained from the other models for $y^+ < 100$. This trend, which can also be seen in the estimates of turbulent kinetic energy, resulted from the added dissipation near the wall and to a lesser extent, from the dissipative nature of the compressibility terms.

The patterns observed in the $M_\infty = 0.2$ results were also seen in the results of the $M_\infty = 1.2$, and 4.0 simulations. This led to the conclusion that the compressibility corrections used by the Grasso & Falconi model have adverse effects on flows at $M \leq 4$. For these reasons, the model was not used in the remainder of this investigation.

**Base Flows**

**Nozzle Flow.** Although Herrin & Dutton's data provide the exit velocity and turbulence intensity distributions near the edge of the circular cylinder, the need for a physical description of the outer edge of the nozzle exit profile prompted the simulation of the entire annular nozzle flow. This approach, which deviates from previous numerical investigations,[7,9] yielded an exit velocity and turbulence distributions which agree with the experimental data near the wall of the circular cylinder as seen in Figure 6.

The streamwise velocity distribution (Figure 6, top) reveals a fully developed turbulent profile at the exit of the nozzle that, although in agreement with the law of the wall, deviates from the experimental results. This discrepancy could be the result of an error in the estimation of the experimental friction velocity ($u_{\tau,exp} = 21.2\ m/s$), which could not be directly measured due to resolution constraints. However, this value was obtained following the method proposed by Sun & Childs.[22] The figure also includes the experimental data normalized by the numerical value for friction velocity ($u_{\tau,num} = 23.3\ m/s$) which improves the agreement between the two data sets.

The bottom part of Figure 6 compares the predicted turbulent kinetic energy at the exit of the nozzle with its measured counterpart. Given that experimentally it was not possible to measure the azimuthal turbulence component, $\overline{v'_\theta}$, inside the nozzle annular channel, the experimental turbulent kinetic energy shown was calculated as

$$k = \frac{1}{2}(\overline{u'}^2 + 2\ \overline{v'_r}^2). \qquad (1)$$

As seen in the figure, even though the shape of the computed kinetic energy function is in agreement with the experimental finding, its magnitude appears to be lower throughout the entire profile even when compared to the experimental data normalized by $u_{\tau,num}$. This difference may be due to mod-

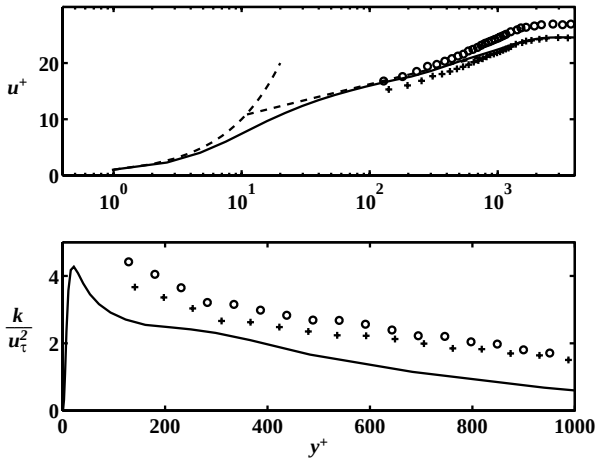


Figure 6. Annular nozzle profiles near the end-corner of the circular cylinder. (Top) streamwise velocity distribution, ——— : present work; - - - : law of the wall; ∘ : Herrin & Dutton's data; + : *corrected* Herrin & Dutton's data. (Bottom) turbulent kinetic energy distribution.

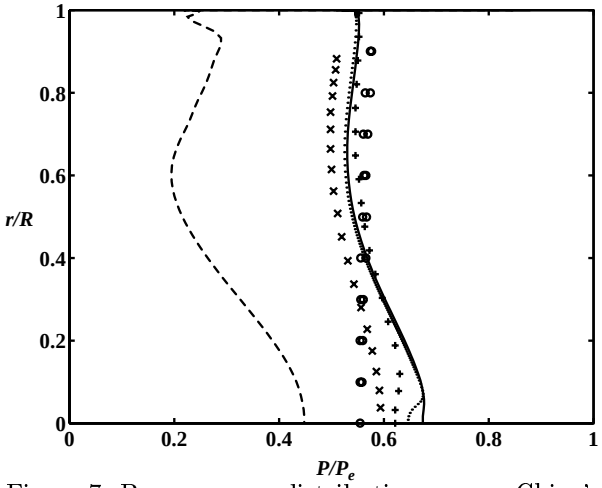


Figure 7. Base pressure distribution. ———: Chien's $k$-$\epsilon$; ·····: Chien's $k$-$\epsilon$, (high resolution); - - -: original Baldwin-Lomax; + : Sahu; × : Tucker & Shyy; ∘ : Herrin & Dutton.

eling errors, although some of the features of the experimental data question its accuracy.

Near the wall ($y^+ < 100$), this annular boundary layer should have the same characteristics as the boundary layer over the flat plate. Consequently, the turbulent kinetic energy should peak at $y^+ \approx 20$ with a value of roughly $4u_\tau$ (see Figure 5, bottom). The peak in the experimental turbulent kinetic energy cannot be determined from the data, given its lack of resolution near the wall; however, if it were extrapolated from the available data, it would be much larger that $4u_\tau$, or would occur at $y^+ \gg 20$.

The experimental data was taken by pushing the circular cylinder outside the confines of the nozzle exit.[23] Based on inviscid theory, this should have no effect on the measurements given that the hyper-extended circular cylinder will remain within the "test diamond" region of the nozzle.[24] However, in a turbulent flow, the hyperextension of the circular cylinder will change the character of the flow in the base region, and this information may propagate upstream through the subsonic portion of the boundary layer. The data of Neves *et al.*[25] indicates that curvature effects on the turbulent intensities are negligible. The observation that the experimental values of $k$ cannot collapse on the accepted values supports the conjecture that the experimental measurements might be in error.

**Turbulence Modeling Effects.** The base flow structure resulting at the design pressure ratio (i.e., $P_e = P_r$) was studied using both the Baldwin-Lomax and Chien's $k$-$\epsilon$ turbulence models. Figure 7 shows a comparison between the experimental base pressure measured by Herrin & Dutton and the numerical predictions of this and two other studies.[7,9] In the figure, it is seen that the Baldwin-Lomax model does not predict the distribution of pressure at the base of the cylinder with satisfactory accuracy. It underpredicts the correct pressure by more than 50%, and the shape of the distribution contains large swings in the pressure as a function of radial distance. The other numerical results are in better agreement with the experiment. Despite slight differences in their numerical algorithms, $k$-$\epsilon$ formulations, grid resolutions and distributions, and boundary conditions, the results do not show much difference among themselves.

The $k$-$\epsilon$ results underpredicted the value of base pressure by 6%, for $r/R > 0.4$, and over-predicted it by 22% at the center of the base. This result is not due to inadequate resolution, which was confirmed by a higher resolution simulation (i.e., $530\times161 + 509\times557 + 674\times249$) which yielded results that only differed from the normal resolution case for $r/R < 0.05$. Further examination of the high resolution data revealed that the resolution discrepancy was produced by a small counter-clockwise recirculation zone at the center of the base, which is not resolved at normal grid resolutions.

Even though the difference between the numerical and experimental predictions of averaged base pressure vanishes when the pressure is integrated

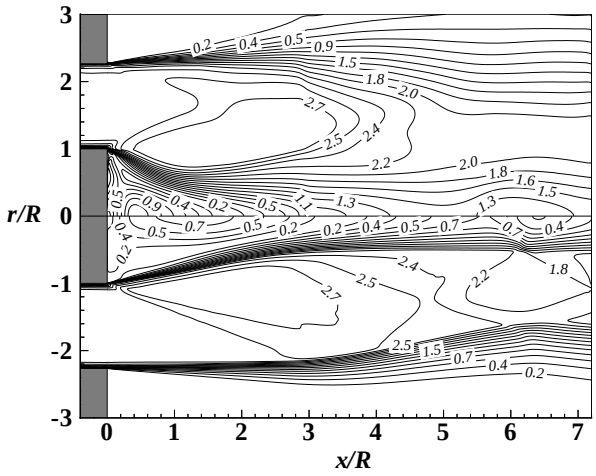


Figure 8. Mach number distribution in the wake of the circular cylinder. (Top half) original Baldwin-Lomax model. (Bottom half) Chien's $k$-$\epsilon$ model.

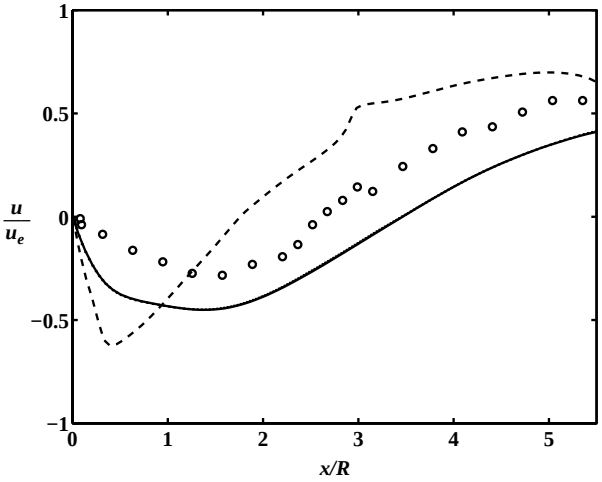


Figure 9. Mean axial velocity distribution in the test section ($u_e = 569\ m/s$). ——— : Chien's $k$-$\epsilon$; ····· : Chien's $k$-$\epsilon$, (high resolution); - - - : original Baldwin-Lomax; ∘ : Herrin & Dutton.

($\bar{P}_{b,exp} = 18.366\ kPa$ vs. $\bar{P}_{b,num} = 17.894\ kPa$, or 2.6% difference), the error in the prediction of base pressure would have been significant for a gas-metal atomization simulation, given that the metal flow is only affected by the pressure at the center of the base. In light of this, one may choose to obtain a value of averaged base pressure and use it to predict the drawing force that the liquid metal experiences during atomization.

Some understanding of the differences between the two model predictions can be achieved by comparing the overall flow structure in the base region. Figure 8 compares the Mach number distributions obtained using the Baldwin-Lomax and Chien's $k$-$\epsilon$ models. As seen in the top half of the figure, the Baldwin-Lomax prediction shows a smaller and shorter recirculation region than the $k$-$\epsilon$ results (bottom half). This is due to a prediction of larger turbulence diffusion across the inner shear layer combined with a larger-than-expected growth of the shear layer. In fact, the Baldwin-Lomax results show a violent and unphysical recirculating flow at the base of the cylinder with the flow along the axis of symmetry becoming supersonic (in the upstream direction) close to the base ($x/R \approx 0.4$). It is this faster moving fluid predicted by the Baldwin-Lomax results that yields the lower values of pressure throughout the face of the cylinder. Furthermore, the deceleration of this reversed supersonic flow along the axis of symmetry is what yields the large spike in pressure near the center of the cylinder. In contrast, the inner shear layer of the $k$-$\epsilon$ simulation spreads at a slower rate and leads to a less violent recirculation region. Consequently, this yields a smoother base pressure distribution.

A similar physical process appears to take place in the outer shear layer of the flow. As seen in the top part of Figure 8, the Baldwin-Lomax model predicts a large amount of diffusion in the outer shear layer, leading to an early spread of the jet. In contrast, the $k$-$\epsilon$ model prescribes a smaller amount of diffusion in this area and, therefore, the outer shear layer spreads only at about half the rate predicted by the Baldwin-Lomax model. Judging from Schlieren pictures of the experiment,[10,19] the spread predicted by the $k$-$\epsilon$ model appears to be more physical than that estimated by the Baldwin-Lomax model.

Figure 9 shows more evidence of the large turbulent diffusion and the early shear layer growth in the Baldwin-Lomax simulation as well as its effects on the overall structure of the wake region. From the figure, it can be seen that the results obtained with the Baldwin-Lomax model exhibited an axial velocity distribution that peaks negatively very close to the base and then recovers too fast, producing an early reattachment at $x/R \approx 1.75$. If the turbulence diffusion across the shear layer had not been overestimated, the recirculation region would have lower velocities and a slower shear layer growth. This would result in greater similarity between the shape of the recirculation region predicted by the simulation and that of the experiment.

The $k$-$\epsilon$ results appear to be in better agreement with the experimental data, but nonetheless, they (a) overpredict the magnitude of the velocity in the

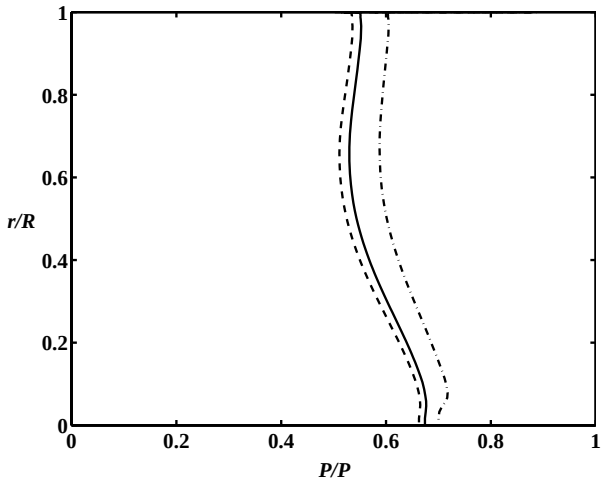

Figure 10. Effect of jet pressure ratio on base pressure distribution. -·-·-: Overexpanded, $P_e/P_r = 0.96$; ——: Design, $P_e/P_r = 1.01$; - - -: Underexpanded, $P_e/P_r = 1.07$.

recirculation region at the base, (b) overpredict the reattachment point by 30%, and (c) underpredict the velocity recovery after the reattachment point. The overprediction in the magnitude of the velocity of the recirculating region is due to an overprediction in the amount of turbulence diffusion across the separated shear layer. Although similar, the turbulence diffusion is not as severe as that seen in Baldwin-Lomax model results. Combined with an underprediction in the growth of the shear layer, this appears to delay reattachment.

**Pressure Ratio Effects.** Given the fundamental interest of this investigation in gas-metal atomization flows, numerical experiments were conducted to determine the effects of jet pressure ratio on the structure of the flow field at the base of the cylinder. Using the same number of grid points, simulations were conducted at pressure ratios, $P_e/P_r$, of: 0.96 (5% overexpanded), 1.01 ($\approx$ design), and 1.07 (5% underexpanded). For all simulations, Chien's $k$-$\epsilon$ model was used.

Figure 10 compares the base pressure distributions for jets at the three pressure ratios considered. From the figure, it can be seen that the shape of the base pressure distribution appears to be independent of the jet pressure ratio, being higher at the center of the cylinder and flatter towards its edge. As expected, the magnitude of the base pressure is inversely proportional to the jet pressure ratio. However, this behavior was found to be nonlinear given that a 5% change in jet pressure ratio yielded a larger change in base pressure for the underexpanded jet than for the overexpanded jet.

Even more interesting is the comparison between the flow field structures obtained for the different jet-pressure ratios. Figure 11 shows static pressure and Mach number distributions for the three jets. The Mach number distributions appear to be very similar in character at all pressure ratios, with an inner shear layer that attaches to the axis of symmetry near $x/R \approx 3.5$. The outer shear layer follows the contours of the pressure diamonds with limited spreading (about $R$ thickness) at distances of $x/R = 7$.

The pressure distributions illustrate many of the flow structures schematically described in Figure 1. For the overexpanded jet (top diagram in Figure 11), a weak shock wave is seen emerging from the outer lip of the nozzle. This shock wave crosses the expansion fan emerging at the end-corner of the circular cylinder and with it, encapsulates the recirculation region at the base of the cylinder. Something very similar is observed in the underexpanded jet (bottom diagram in Figure 11), although the shock wave is replaced by an expansion wave that emanates from the outer lip of the nozzle. In the design jet (center diagram in Figure 11), there is neither a shock nor an expansion wave originating at the outer lip of the nozzle (the lines on this region are due to noise in the contouring algorithm) and therefore, there is no encapsulation of the base flow region by wave structures. The size of the recirculation region appears to be directly proportional to the jet pressure ratio.

Further downstream, the jet structures appear to be very similar. The expansion waves emanating from the end-corner of the cylinder are reflected as compression waves by the outer shear layer. They interact with the compression waves created in the reattachment zone at the axis of symmetry and lead to two shock waves from different families which then initiate a dual diamond structure similar to that seen in annular supersonic jets.

For all three pressure ratios studied, some of the structures associated with the inner shear layer remain for distances of up to $x/R = 9$ (see Figure 12). This continuation of the inner shear layer prevents the downward propagating shock wave from reaching the axis of symmetry, reflecting it at $x/R \approx 6.2$ and $r/R \approx 0.5$. This process totally bypasses the formation of the Mach reflection reported in other base flow investigations.[2] Meanwhile, the upward propagating shock wave reflects from the outer shear layer at $x/R \approx 6.4$ resulting in an expansion fan

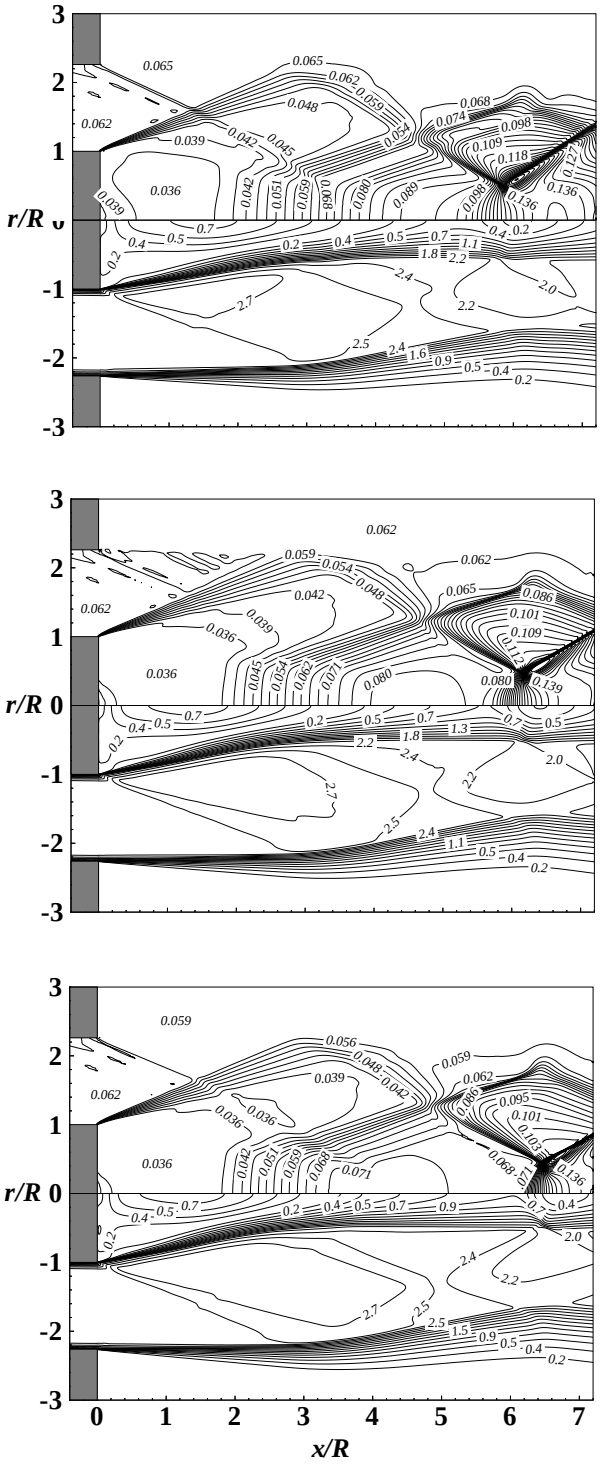


Figure 11. Effect of jet pressure ratio on pressure ($P/P_o$, upper halves) and Mach number (lower halves) distributions in the wake of the circular cylinder. (Top) overexpanded, $P_e/P_r = 0.96$; (Center) design, $P_e/P_r = 1.01$; (Bottom) underexpanded, $P_e/P_r = 1.07$.

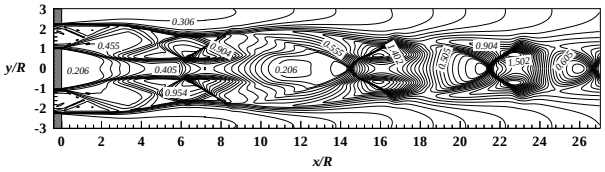


Figure 12. Density distribution in the wake of a circular cylinder at design pressure ratio ($\rho/\rho_{ref}$, $\rho_{ref} = 1.293\ kg/m^3$).

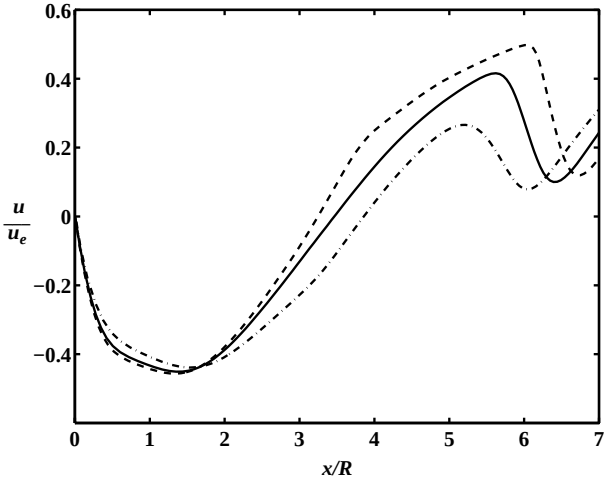


Figure 13. Effect of jet pressure ratio on mean axial velocity distribution in the test section ($u_e = 569\ m/s$). -·-·- : Overexpanded, $P_e/P_r = 0.96$; ——— : Design, $P_e/P_r = 1.01$; - - - : Underexpanded, $P_e/P_r = 1.07$.

that is absorbed by the continuation of the inner shear layer in the area from $x/R \approx 8$ to $x/R \approx 9.2$. From this location on, the jet loses its dual diamond structure associated with its annular formation and instead, exhibits a single barrel-shock chain similar to that seen in regular supersonic jets.

Figure 13 shows the effects of pressure ratio on the axial velocity distribution of the jet. For $x/R < 2$, the velocity distribution remains almost unchanged, peaking negatively at $x/R \approx 1.5$. However, for larger axial distances, the length of the jet structures is directly proportional to the pressure ratio.

Contrary to the other structures, the reattachment point moves upstream in the underexpanded jet and downstream in the overexpanded jet. This behavior results from the strength of the expansion fan at the end-corner of the cylinder. This expansion fan deflects the flow in the underexpanded jet at a sharper angle towards the axis of symmetry than it does in the overexpanded jet. The fact that the magnitude of the change in the location of reat-

tachment is almost the same for both off-design jets indicates that the relation between pressure ratio and reattachment location is linear for this range of pressure ratios.

At larger axial distances ($5 < x/R < 7$), the axial velocity peaks for the first time. The deceleration that follows tends towards the discontinuity associated with a Mach reflection as the pressure ratio is increased. In fact, the peak in axial velocity only attains a Mach number of 0.5 for the overexpanded jet, while it reaches $M = 0.9$ for the underexpanded case. Further increases in the pressure ratio force the inner shear layer closer to the axis of symmetry, resulting in the formation of a Mach reflection.

## Conclusions

The strengths and limitations of the NPARC code when used to model supersonic based flows have been assessed. Simulations of compressible boundary layers demonstrated deficiencies in the NPARC's implementation of the Baldwin-Lomax turbulence model which yields discontinuous eddy viscosity distributions in wall bounded flows and no turbulence in free shear flows. With the addition of the wake model proposed by Baldwin & Lomax and a trapezoidal filter, the model could be useful in the computation of complex flows.

The $k$-$\epsilon$ model by Grasso & Falconi yielded unsatisfactory results for boundary layers with free stream Mach numbers in the 0.2 to 4.0 range. The problems seen with this model appear to be due to large values of turbulent dissipation near the wall and the dissipative nature of the extra compressibility terms. With attention to discretization details, the $k$-$\epsilon$ model by Chien rendered results in agreement with DNS data for boundary layer flows and with experiments involving base flows.

The base flow results obtained in this investigation are in good agreement with the experimental data and results of previous numerical investigations. Local values of base pressure were found to differ from their experimental counterparts by as much as 22%. However, the averaged value of base pressure was found to be in agreement with the experiment. The location of the reattachment point was overpredicted by 30% due to a smaller than expected growth of the inner shear layer.

The magnitude of the base pressure was found to be inversely proportional to the jet pressure ratio, even though the function appears to be nonlinear. The axial location of jet structures were found to directly proportional to the jet pressure ratio. However, the location of the reattachment point was found to follow the inverse behavior. This effect was shown to be associated with the strength of the expansion process at the end-corner of the circular cylinder which deflects the inner shear layer at sharper angles for higher pressure ratios.

The results indicate that there are four distinct flow regimes that these base flows undergo as a function of jet pressure ratio. At low pressure ratios in the overexpanded regime, the jet exhibits an annular structure which leads to an open base region with a pressure close to that of the receiving chamber. At pressure ratios near the design condition, the inner shear layer reaches the axis of symmetry closing the base region. However, a subsonic core remains and this perpetuates the annular wave structure of the jet. At higher pressure ratios, the core of the jet attains supersonic velocities and leads to the formation of a Mach reflection downstream of the reattachment point. This Mach reflection changes the character of the jet from annular to circular. Further increases in the jet pressure ratio lead to the replacement of the Mach reflection by a simple reflection at the axis of symmetry.

The methodology used in this investigation should enable the use of the NPARC code for the simulation of the gas-only flow fields in close-coupled gas-metal atomizers that have geometries similar to that studied here.

## Acknowledgements

This investigation was sponsored by the Chemical Science and Technology Laboratory of the National Institute of Standards and Technology (NIST) under the guidance of George E. Mattingly and Gregory J. Rosasco. Computational support was provided by the High Performance Systems and Service Division at NIST. In addition, enlightening discussions with Jeff L. Herrin of NASA-Langley, Greg D. Power of Sverdrup Technology, Inc., and Nicholas J. Georgiadis of NASA-Lewis are gratefully acknowledged.

## References

[1] Mueller, T. J., "Determination of the Turbulent Base Pressure in Supersonic Axisymmetric Flow," *Journal of Spacecraft and Rockets*, Vol. 5, No. 1, 1968, pp. 101–107.

[2] Sule, W. P., and Mueller, T. J., "Annular Truncated Plug Nozzle Flowfield and Base Pressure Characteristics," *Journal of Spacecraft and Rockets*, Vol. 10, No. 11, 1973, pp. 689–695.

[3] Mueller, T. J., "The Role of Flow Visualization in the Study of Afterbody and Base Flows: A Review," *Experiments in Fluids*, Vol. 3, 1985, pp. 61–70.

[4] Mikhail, A. G., Hankey, W. L., and Shang, J. S., "Computation of a Supersonic Flow Past an Axisymmetric Nozzle Boattail with Jet Exhaust," *AIAA Journal*, Vol. 18, No. 8, 1980, pp. 869–875.

[5] Sahu, J., Nietubicz, C. J., and Steger, J. L., "Navier-Stokes Computations of Projectile Base Flow with and without Mass Injection," *AIAA Journal*, Vol. 23, No. 9, 1985, pp. 1348–1355.

[6] Sahu, J., "Three-Dimensional Base-Flow Calculation for a Projectile at Transonic Velocity," *AIAA Journal*, Vol. 27, No. 2, 1989, pp. 138–139.

[7] Sahu, J., "Numerical Computations of Supersonic Base Flow With Special Emphasis on Turbulence Modeling," *AIAA Journal*, Vol. 32, No. 7, 1994, pp. 1547–1549.

[8] Peace, A. J., "Turbulent Flow Predictions for Afterbody/Nozzle Geometries Including Base Effects," *Journal of Propulsion and Power*, Vol. 7, No. 3, 1991, pp. 396–403.

[9] Tucker, P. K., and Shyy W., "A Numerical Analysis of Supersonic Flow Over an Axisymmetric Afterbody," AIAA Paper 93–2347, June 1993.

[10] Herrin, J. L. and Dutton, J. C., "Supersonic Base Flow Experiments in the Near Wake of a Cylindrical Afterbody," *AIAA Journal*, Vol. 32, No. 1, 1994, pp. 77–83.

[11] Baldwin, B. S. and Lomax, H., "Thin Layer Approximation and Algebraic Model for Separated Turbulent Flows," AIAA Paper 78–257, Jan. 1978.

[12] Chien K.-Y., "Predictions of Channel and Boundary-Layer Flows with a Low-Reynolds-Number Turbulence Model," *AIAA Journal*, Vol. 20, No. 1, 1982, pp. 33–38.

[13] Georgiadis, N. J., Dudek, J. C., and Tierney, T. P., "Grid Resolution and Turbulent Inflow Boundary Condition Recommendations for NPARC Calculations," AIAA Paper 95–2613, July 1995.

[14] Grasso, F. and Falconi, D., "High-Speed Turbulence Modeling of Shock-Wave/Boundary-Layer Interaction," *AIAA Journal*, Vol. 31, No. 7, 1993, pp. 1199–1206.

[15] Cooper, G. K. and Sirbaugh, J. R., "PARC Code: Theory and Usage," Sverdrup Technology, Inc., Arnold Engineering Development Center, AEDC–TR–89–15, Arnold AFB, TN, Dec. 1989.

[16] Pulliam, T. H. and Steger, J. L., "Implicit Finite-Difference Simulation of Three-Dimensional Compressible Flows," *AIAA Journal,* Vol. 18, No. 2, 1980, pp. 159–167.

[17] Sahu, J. and Danberg, J. E., "Navier-Stokes Computations of Transonic Flows with a Two-Equation Turbulence Model," *AIAA Journal*, Vol. 24, No. 11, 1986, pp. 1744–1751.

[18] Lilienthal, P. F., Brink, D. F., and Addy, A. L., "Experimental Program for the Study of Supersonic and Transonic Axisymmetric Base-Pressure Problems," Dept. of Mech. and Ind. Eng., Univ. of Illinois at Urbana-Champaign, Urbana, IL, July 1970.

[19] Sauter, J. M. and Dutton, J. C., "Design of an Axisymmetric Supersonic Wind Tunnel and Experimental Study of Supersonic, Power-Off Base Flow Phenomena," Dept. of Mech. and Ind. Eng., Univ. of Illinois at Urbana-Champaign, UILU ENG 89–4002, Urbana, IL, Mar. 1989.

[20] Davies, C. B. and Venkatapathy, E. "Application of a Solution Adaptive Grid Scheme to Complex Three-Dimensional Flows," *AIAA Journal*, Vol. 30, No. 9, 1992, pp. 2227–2233.

[21] Spalart, P. R., "Direct Simulation of a Turbulent Boundary Layer up to $R_\theta = 1410$," *J. Fluid Mech.*, Vol. 187, 1988, pp. 61–98.

[22] Sun, C. C., and Childs, M. E., "A Modified Wall Wake Velocity Profile for Turbulent Compressible Boundary Layers," *Journal of Aircraft*, Vol. 10, No. 6, 1973, pp. 381–383.

[23] Herrin, J. L., private communication.

[24] Pankhurst, R. C., and Holder, D. W., *Wind-Tunnel Technique*, Sir Isaac Pitman & Sons, Ltd., London, 1952, pp. 105–112.

[25] Neves, J. C., Moin, P., and Mosser, R. D.,"Effects of Convex Transverse Curvature on Wall-Bounded Turbulence. Part 1. The Velocity and Vorticity," *J. Fluid Mech.*, Vol. 272, 1988, pp. 349–381.